THE JOURNAL OF BIOLOGICAL CHEMISTRY VOL. 290, NO. 34, pp. 21032–21041, August 21, 2015

Aerobic Growth of *Escherichia coli* Is Reduced, and ATP Synthesis Is Selectively Inhibited when Five C-terminal Residues Are Deleted from the ϵ Subunit of ATP Synthase*

Received for publication, May 13, 2015, and in revised form, June 19, 2015 Published, JBC Papers in Press, July 9, 2015, DOI 10.1074/jbc.M115.665059

Naman B. Shah[1] **and Thomas M. Duncan**[2]

From the Department of Biochemistry and Molecular Biology, State University of New York, Upstate Medical University, Syracuse, New York 13210

Background: Bacterial ATP synthases are autoinhibited by subunit ϵ.
Results: Altering the regulatory interactions of ϵ increases inhibition of ATP synthesis and reduces respiratory growth of *E. coli*.
Conclusion: The ϵ subunit can have distinct regulatory interactions during ATP synthesis *versus* hydrolysis.
Significance: Inhibition by ϵ provides a bacteria-specific means to target ATP synthase for antibiotic development.

F-type ATP synthases are rotary nanomotor enzymes involved in cellular energy metabolism in eukaryotes and eubacteria. The ATP synthase from Gram-positive and -negative model bacteria can be autoinhibited by the C-terminal domain of its ϵ subunit (ϵCTD), but the importance of ϵ inhibition *in vivo* is unclear. Functional rotation is thought to be blocked by insertion of the latter half of the ϵCTD into the central cavity of the catalytic complex (F_1). In the inhibited state of the *Escherichia coli* enzyme, the final segment of ϵCTD is deeply buried but has few specific interactions with other subunits. This region of the ϵCTD is variable or absent in other bacteria that exhibit strong ϵ-inhibition *in vitro*. Here, genetically deleting the last five residues of the ϵCTD (ϵΔ5) caused a greater defect in respiratory growth than did the complete absence of the ϵCTD. Isolated membranes with ϵΔ5 generated proton-motive force by respiration as effectively as with wild-type ϵ but showed a nearly 3-fold decrease in ATP synthesis rate. In contrast, the ϵΔ5 truncation did not change the intrinsic rate of ATP hydrolysis with membranes. Further, the ϵΔ5 subunit retained high affinity for isolated F_1 but reduced the maximal inhibition of F_1-ATPase by ϵ from >90% to ~20%. The results suggest that the ϵCTD has distinct regulatory interactions with F_1 when rotary catalysis operates in opposite directions for the hydrolysis or synthesis of ATP.

The F-type ATP synthase is a self-contained rotary motor enzyme that is critical for efficient energy metabolism in eukaryotes and eubacteria (1–4). It is composed of a membrane-embedded F_0 complex that catalyzes proton transport and an external F_1 complex with three cooperative catalytic nucleotide-binding sites, and all bacterial subunits are conserved in the eukaryotic enzymes of mitochondria and chloroplasts (3, 5). So far, no complete high resolution structures have been determined for F_0, but it is well accepted that the mechanism of proton transport involves rotation of a central ring of ***c***-subunits (***c***-ring) relative to two half-channels at the interface of the *c*-ring with subunit ***a*** (2–4). The structural assembly of F_1 (Fig. 1*A*) includes a hexamer of alternating α and β subunits that surround the central rotor stalk region of the asymmetric γ subunit. The lower region of γ and the N-terminal domain (ϵNTD)[3] of the ϵ subunit form the central rotor stalk that connects with the rotary ***c***-ring of F_0, and although structural details are still lacking, a peripheral stator stalk connection is formed by F_1 subunit δ and the b_2 dimer of F_0 (6). For ATP synthesis, proton motive force (PMF) generated by the electron transport chain drives rotation of the ***c***-ring, which is coupled with the rotation of γ within F_1. Rotation of the asymmetric γ subunit helps drive conformational changes in α and β subunits that are crucial for cooperative, alternating catalysis at the three catalytic nucleotide binding sites located mainly on the β subunits.

ATP synthases can also rotate in the reverse direction by hydrolyzing ATP to generate PMF. In mitochondria, this ATPase-driven proton pumping can be blocked by a mitochondria-specific inhibitor protein called IF_1 (7, 8). In contrast, many bacterial ATP synthases can be autoinhibited by the C-terminal domain (CTD) of the ϵ subunit (2, 9), which can inhibit both synthesis and hydrolysis of ATP (10, 11). The ϵCTD can transition between at least two observed states: a compact conformation (ϵ_C; Fig. 1*C*) that allows coupled functions (12), and an extended conformation (ϵ_X; Fig. 1*A*) (13) that likely corresponds to an inactive or paused state of the enzyme (14, 15). In the ϵ_C state, the two α-helices of the ϵCTD form a hairpin coiled coil that packs against the ϵNTD, as observed

* This work was supported, in whole or in part, by National Institutes of Health Grant R01GM083088. The authors declare that they have no conflicts of interest with the contents of this article.
[1] Present address: Dept. of Microbiology and Immunology, Cornell University College of Veterinary Medicine, C5 141 Veterinary Medical Center, Ithaca, NY 14853.
[2] To whom correspondence should be addressed: Dept. of Biochemistry and Molecular Biology, SUNY Upstate Medical University, 750 East Adams St., Syracuse, NY 13210. Tel.: 315-464-8711; Fax: 315-464-8750; E-mail: duncant@upstate.edu.

[3] The abbreviations used are: NTD, N-terminal domain; PMF, proton-motive force; CTD, C-terminal domain; FCCP, carbonyl cyanide 4-(trifluoromethoxy)phenylhydrazone; ACMA, 9-amino-6-chloro-2-methoxyacridine; LDAO, *N*,*N*-dimethyldodecylamine *N*-oxide; DCCD, *N*,*N*′-dicyclohexylcarbodiimide; AMPPNP, adenosine 5′-(β,γ-imido)triphosphate; Bap, biotinylation acceptor peptide; BLI, biolayer interferometry.

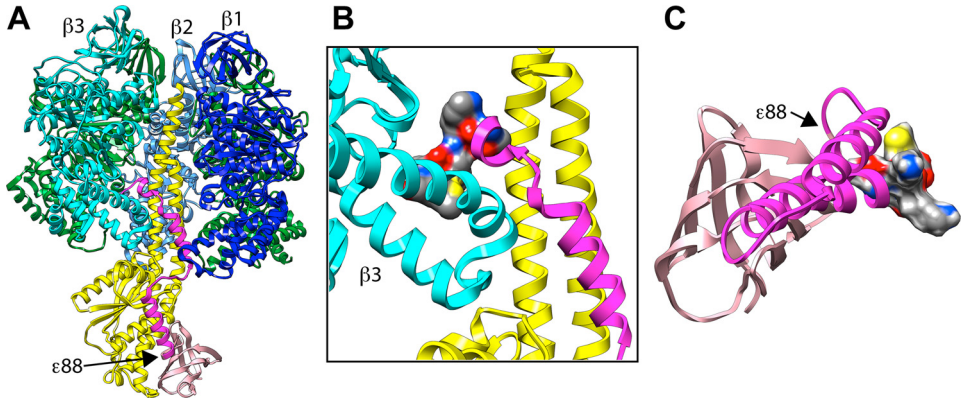

FIGURE 1. **Location of the ϵ subunit CTD and five C-terminal residues in two known conformations.** *A*, ribbon diagram of an ϵ-inhibited structure of the F_1 catalytic complex from *E. coli* ATP synthase (13). The hexameric "head" is composed of three catalytic β subunits (shades of *blue* and *numbered*) that alternate with three α subunits (*green*); the frontmost α is omitted to reveal the portions of subunit γ (*yellow*) and of the ϵCTD (*magenta*) that are buried in the central cavity of the $\alpha_3\beta_3$ hexamer. The "foot" of γ and the ϵNTD (*pink*) form the rotor connection to the *c*-ring of F_0. *B*, magnified view of the ϵCTD segment that is buried in the central cavity of F_1. The five terminal residues of ϵ, ϵ134–138, are surface-rendered, colored by element, and contact only γ (*yellow*) and β3 (*blue*). Contacts with β3 account for 78% of the buried surface area lost with the ϵΔ5 truncation. *C*, ribbon diagram of the compact conformation (ϵ_C) of isolated ϵ (16), with the ϵNTD oriented as in *A*; of the five terminal residues, ϵ134–138 (surface rendered as in *B*), only ϵT134 contacts the ϵNTD. In *A* and *C*, *arrows* mark the position of ϵ88, the point at which the ϵCTD is truncated for the ϵ88stop mutant. All proteins were rendered with Chimera (77).

with isolated ϵ from two species (16, 17) and in one bacterial F_1 structure (18). In mitochondrial F_1 structures, the ϵ homolog appears to be locked in the ϵ_C conformation by a unique mitochondrial subunit (19). Thus far, an extended state of the ϵCTD has only been observed within the enzyme in a crystal structure of *Escherichia coli* F_1 (13), in which the latter half of the ϵCTD inserts into the central cavity of F_1 and has extensive contacts with other subunits. The second α-helix of the ϵ_X state (ϵ112–125) contacts five other subunits, with apparent H-bonds and/or salt bridges to α1, α2, β1, and γ subunits. The terminal segment of ϵCTD (ϵ126–138) was called the ϵ-hook in the ϵ_X state, because it bends around γ and "hooks" the CTD of another catalytic subunit, β3 (Fig. 1*B*). The ϵ-hook buries extensive surface area within F_1 but has minimal specific interactions, with perhaps one H-bond (ϵIle^{131} amide to β3-Asp^{372} side chain). The final C-terminal segment of ϵ varies significantly in sequence and length between diverse bacterial species (9). High resolution structures have been determined for bacterial ϵ from two other species, *Bacillus PS3* (17) and *Caldalkalibacillus thermarum* TA2.A1 (18); both superimpose well with the ϵ_C conformation of *E. coli* ϵ but are shorter at the C terminus by 4 and 3 residues, respectively. Despite this, the activity of each ATP synthase can be strongly inhibited by the shorter ϵCTD (10, 20, 21). Thus, we postulated that the final segment of the ϵ-hook might be dispensable or even destabilizing for inhibition by the ϵCTD. Inhibition by ϵ is not essential for respiratory growth of *E. coli*, because significant growth on a nonfermentable carbon source can be achieved with the entire ϵCTD genetically truncated (22, 23). Interestingly, however, an early mutagenic study with *E. coli* found that combined deletion of 4 C-terminal and 15 N-terminal residues disrupted growth by oxidative phosphorylation, whereas the N-terminal truncation alone did not (24). In this study, we genetically deleted just the final five amino acids of ϵCTD (ϵ134–138) to generate an *E. coli* ϵΔ5 mutant. Growth on a nonfermentable carbon source was reduced ~60% by ϵΔ5, whereas complete deletion of the ϵCTD (ϵ88stop) reduced growth by ~20%. With isolated membranes, ϵΔ5 reduced the ATP synthesis rate by >2.7-fold, but did not alter ϵ inhibition of ATPase activity. Thus, the ϵΔ5 truncation has distinct effects on ATP synthesis *versus* hydrolysis. Since a new class of effective antibacterial agents has been found to target the ATP synthase (25), our results show that regulation by the ϵCTD provides a bacteria-specific target for future development of antibacterials against the ATP synthase.

Experimental Procedures

Plasmids and Mutagenesis—Plasmid p3DC (26), which encodes subunits β and ϵ, was used as template to truncate the terminal five amino acids of ϵCTD via site-directed mutagenesis (27). Primer 5′-CAGCTGCGCGTTATCGAGTTG**TA-ATAA**AAAGCGATGTAACACCGGC-3′ (mutations underlined) was used to replace codons for ϵThr^{134}/Lys^{135} with two ochre stop codons (bold type). DNA sequencing (Upstate Medical University core facility) was used to confirm that only the desired mutations were created. DNA encoding ϵ with the stop codons (ϵΔ5) was extracted in a NdeI-XbaI restriction fragment and used to replace the corresponding fragment of pAU1 (26) to obtain pAU1ϵΔ5. The NdeI-XbaI fragment was also used to move ϵΔ5 into pBKH8 (15), creating pBKH8ϵΔ5. The ϵ88stop truncation was also moved in a NdeI-XbaI fragment from pBKH9 (15) into pAU1. The βM209L mutation was originally a gift from A. E. Senior (28) and was transferred to pAU1 in a SacI-EagI fragment.

Phenotypic Assay for Respiratory Growth—F_0F_1, either WT or with the mutants noted (Fig. 2 and Table 1), was expressed from the *atp* operon on low copy plasmid pAU1. For most phenotypic growth tests, pAU1 constructs were transformed into strain LE392Δ(*atpI-C*) (29). Individual bacterial colonies were inoculated into 10 ml of Luria Bertani broth (LB; Lennox type, Sigma Aldrich) + ampicillin (0.1 mg/ml) and grown overnight at 37 °C, with shaking at 200 rpm in a 125-ml Erlenmeyer flask. Cells were then diluted into 10 ml of fresh LB + ampicillin to obtain an A_{600} of 0.1. When growth reached A_{600} ~0.8, cells were diluted 100-fold into defined minimal salts medium (30) including 1 mM $MgSO_4$, 0.1% (v/v) trace elements (30), 0.06%

cas-amino acids (BD Difco), 6 μM thiamine, 0.1 mg/ml ampicillin, 50 μg/ml methionine, and 30 mM succinate as the nonfermentable carbon source. Growth at 37 °C was measured with 0.4 ml of culture per well in a 48-well transparent microtiter plate with lid (catalog no. 677102; Greiner Bio-one), with triplicate samples for each distinct pAU1 construct. Growth was monitored every 15 min by A_{600}, using a plate reader (Biotek Synergy HT or TECAN Infinite F200). Plates were shaken at 88.6 rpm (TECAN) or at "slow" setting (Biotek) for 20–30 h. Some assays were repeated with the same plasmids in a distinct *atp*-deletion strain, DK8 (31), so the defined growth medium included 0.3 mM isoleucine and valine and omitted methionine. The DK8 strains showed less stringent differences in growth between WT and negative controls in initial tests. For more consistent performance, defined medium for DK8 had reduced cas-amino acids (0.03%) and succinate (6 mM). Also, to reduce carryover of LB, DK8 cells from starter cultures were sedimented and resuspended with defined medium before final dilution into defined medium for the assay.

Isolation of Inverted Membrane Vesicles—Strain LE392Δ (*atpI-C*) containing pAU1 (WT or ϵ mutants) was inoculated from individual colonies into 10 ml of LB + ampicillin (0.1 mg/ml) and grown overnight in a 125-ml Erlenmeyer flask at 37 °C with shaking (200 rpm). Cells were then diluted into 2 liters of defined minimal salts medium (30) to obtain an A_{600} of ~0.05. Additions were as noted earlier except that 30 mM glucose and 1% glycerol were the carbon sources. The cells were grown at 37 °C with constant aeration and were harvested during logarithmic growth phase. Inverted membrane vesicles (membranes) were prepared as described before (32), but with a final exchange into 50 mM MOPS-Tris, 10% (v/v) glycerol, 5 mM magnesium acetate, pH 7.5.

Expression and Purification of Proteins—WT-F_0F_1 was expressed, and F_1 was released from membranes, purified, and depleted of subunits δ and ϵ as before (13, 15). For expression of biotinylated ϵ as an MBP-Bap-ϵ fusion protein, pBKH8 (WT or ϵΔ5) was transformed into strain DH5α (33). Biotinylated ϵ (WT or ϵΔ5) was expressed and purified as before (15). Concentrations and purity of proteins were determined by a modified Lowry assay (34) and SDS-PAGE (35).

Detection of F_0F_1 Content in Membrane Vesicles by Immunoblotting—Membrane samples (at least two amounts each) and known amounts of purified F_1 were subjected to SDS-PAGE (35) on precast 4–20% gradient polyacrylamide gels (Bio-Rad) at 200 V for 33 min. Proteins were then transferred to a polyvinylidene difluoride membrane (Invitrogen) in a Bio-Rad Mini Trans-Blot cell at 200 mA for 1 h using 1× electrophoresis buffer (35) + 10% (v/v) methanol. The blot was blocked with TBST (10 mM Tris-Cl, 150 mM NaCl, pH 8, 0.05% Tween 20) + 5% (w/v) nonfat dried milk and then washed three times for 5 min each with TBST (0.3 M NaCl total). The blot was then incubated for 1 h with the primary rabbit anti-β antibody (1:200) in TBST +BSA (10 mg/ml); this anti-β antibody (antibody AS05-85; Agrisera) was previously tested for this purpose with *E. coli* membranes (36). The blot was washed three times as above, followed by 1 h with a fluorescent goat anti-rabbit secondary antibody (antibody 35553; Thermo Scientific), 1:1000 dilution in TBST +BSA. After three final washes as above, the blot was air-dried, and fluorescence was detected on a Typhoon 9410 imager (GE Healthcare Life Sciences) with a 532-nm laser and 526-nm short pass filter. Signals for β from known amounts of F_1 provided a linear response range that was used to quantify the amount of β in different membrane samples.

ATP Hydrolysis—ATP hydrolysis rates were measured at 30 °C with a coupled enzymes assay (37) as described (15). Assays with membranes contained 5 mM magnesium acetate and 2 mM ATP, 5 mM KCN to inhibit NADH oxidation by the electron transport chain and 5 μM FCCP as uncoupler to prevent generation of PMF. Assays to measure ϵ inhibition of isolated F_1(-δϵ) included preincubation of F_1(-δϵ) with ϵ, 2 mM ATP, and 0.1 mM EDTA, and the values for K_I and maximal inhibition with Bap-ϵΔ5 were determined as before for WT-ϵ and ϵ88stop (15). Assays of NADH oxidation by the electron transport chain were done with the same conditions but without ATP or coupling enzymes, and ±KCN; oxidation rates were >88% inhibited by KCN, confirming that most NADH oxidation was through the electron transport chain in all membranes.

ATP Synthesis—Assays of ATP synthesis by membranes were modified from (38). The membranes were diluted to 0.105 mg/ml final in 1910 μl of synthesis reaction buffer (50 mM MOPS-Tris, pH 7.5 + 10 mM magnesium acetate) in a 1 × 1-cm cuvette. Aeration was achieved throughout the assay by stirring with a cylindrical magnetic stirrer with cross-cut channels. Reactions were done at ambient temperature (~22 °C). Membranes were allowed to equilibrate for 2 min after dilution into the cuvette. NADH (50 μl of 0.1 M stock) was added to 2.5 mM final concentration, and after 1 min to establish PMF, ATP synthesis was started by adding 40 μl of ADP/P_i mixture to obtain 1 mM ADP and 3 mM P_i final (total assay volume, 2.0 ml). Over 4 min, 100 μl of reaction was withdrawn at 1-min intervals and added to 400 μl of ice-cold stop solution (1% TCA, 2 mM EDTA) with vortexing, and the quenched samples were kept on ice. For each membrane sample tested, a control time course was done with 10 μM FCCP present to prevent PMF formation; this corrected for (i) minimal ATP synthesis from ADP by contaminating pyruvate kinase and (ii) residual ATP in the assay (primarily from the ADP stock). For each quenched sample in duplicate, 10 μl was added to 390 μl of ice-cold luciferase assay buffer (0.1 M Tris acetate, 2 mM EDTA, pH 7.5). Samples of ATP standards were treated with stop solution and diluted as above to provide a linear response over 0.25–12 pmol in the final measurement. Samples could be frozen at this point, if needed. For each neutralized sample, 100 μl was transferred to a well of a white, opaque 96-well microtiter plate (catalog no. 236108; Nunc), which was then equilibrated to ambient temperature. The plate was placed in a Synergy HT microplate reader (Biotek) equipped with autoinjectors. For each sequential sample well, 50 μl of luciferase reagent (ATP bioluminescence assay kit CLS II; Roche Diagnostics) was injected, and luminescence was measured for 10 s (top path, no emission filter; integration, 1 s; gain, 135). The rates of synthesis for control samples (+FCCP) were minimal and were subtracted from rates with energized membranes to obtain ATP synthesis rates caused by the ATP synthase. All membranes assayed showed linear rates of ATP syn-

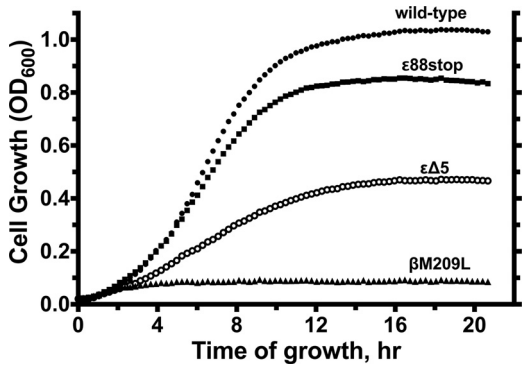

FIGURE 2. **Phenotypic assay for growth of *E. coli* by respiration.** LE392(Δ*atpI-C*) cells expressing F_0F_1 from pAU1were grown on defined medium with succinate as the sole carbon source. The ϵ subunit expressed was WT (●), ϵ88stop (■), or ϵΔ5 (○); a negative control expressed WT-ϵ but catalytically defective βM209L subunit (▲). Each data set is averaged from triplicate cultures grown in parallel; analyses for multiple experiments are in Table 1.

TABLE 1

Effect of ϵCTD truncations on aerobic growth on succinate

The values with ranges are means ±S.E. with the number of independent experiments for each assay noted in parentheses.

Strain	Growth yield	Growth rate	Relative F_0F_1 content[a]
	% of WT	A_{600}/*h*	
WT	100 ±9 (5)	0.2 ± 0.01 (5)	1
ϵ88stop	78 ±13 (4)	0.14 ± 0.03 (4)	0.23 ± 0.006 (2)
ϵΔ5	38 ±4 (6)	0.08 ± 0.01 (6)	0.54 ± 0.001 (2)
βM209L	4 ± 2 (3)	NS[b]	ND[c]

[a] Amounts of F_0F_1 in membrane were quantified by anti-β antibody (Experimental Procedures). The values were normalized relative to WT.
[b] NS, not significant.
[c] ND, not determined, but previously measured as equivalent to WT (28).

thesis over the assay period (all linear fits used had R^2 values of >0.98).

Proton Pumping—Proton pumping activity of membranes was measured by monitoring fluorescence quenching of ACMA, which reflects ΔpH (39). Membranes were diluted to 0.1 mg/ml in assay buffer (20 mM MOPS-Tris, pH 7.5, 50 mM KCl, 5 mM magnesium acetate) + 1 μM ACMA and equilibrated for ~9 min, and the assay was started by adding NADH or ATP to drive proton pumping. Total assay volume was 2 ml in a 1 × 1-cm fluorescence cuvette, and aeration was maintained by stirring, as in the ATP synthesis assays. Assays were done at 30 °C on a Fluoromax-4 or Fluorolog-3 (Horiba Scientific) with excitation/emission wavelengths (nm) of 430/560, excitation/emission slits of 5/4 nm, gratings set at 1200, integration time of 0.5 s, and interval time of 7.5 s. For WT and each ϵ mutant, at least two separate preparations of membranes from different cell growths were tested.

BioLayer Interferometry (BLI)—Biolayer interferometry was used to study interactions between isolated F_1(-δϵ) and biotinylated ϵ variants. Experiments were done in an Octet RED system (Pall ForteBio) as described (15, 40).

Results

Effects of ϵCTD Truncations on Aerobic Growth—To observe whether ϵCTD truncations affect *in vivo* function of the ATP synthase, bacteria expressing WT or mutant forms of F_0F_1 were grown with a nonfermentable carbon source, succinate, so growth required oxidative phosphorylation (41). As shown in Fig. 2 and Table 1, growth on succinate was negligible for cells expressing F_0F_1 with a control mutation, βM209L, which allows assembly of normal levels of ATP synthase on the membrane but renders it essentially inactive (28, 42). Deletion of the entire ϵCTD (ϵ88stop) reduced respiratory growth yield only ~20%, with little effect on growth rate. This is consistent with another group's study in which ϵ88stop allowed respiratory growth on acetate and caused a minimal decrease in growth yield on limiting glucose (22). In contrast, deleting only five C-terminal amino acids from ϵ (ϵΔ5) reduced growth yield and growth rate (Table 1) by ~60%. Growth assays were repeated with the same plasmids expressed in a distinct Δ*atp*-operon host strain, DK8. Initially, the DK8 strains showed less robust differences in phenotypic growth, possibly because of greater C_4-dicarboxylate transporter activity (43). For subsequent assays, succinate concentration was reduced 5-fold, and results were similar to the effects of mutations seen in Table 1 and Fig. 2 (DK8 growth yields relative to WT: ϵ88stop, 95%; ϵΔ5, 46%; βM209L, 9%). The greater phenotypic defect of ϵΔ5 was not simply due to poor expression or assembly of F_0F_1 because ϵΔ5 membranes showed higher F_0F_1 content than for ϵ88stop (Table 1). Thus, the entire ϵCTD can be removed with minimal effects, but the small ϵΔ5 truncation perturbs the regulatory interactions of ϵCTD so that the capacity for *in vivo* oxidative phosphorylation is significantly degraded.

Effects of ϵCTD Truncations on in Vitro Functions of Membrane-bound ATP Synthase—To further examine why ϵΔ5 is more deleterious than ϵ88stop *in vivo*, membranes were isolated and tested for effects of ϵCTD truncations on activities of F_0F_1 *in vitro*. Membrane ATP hydrolysis was measured with excess uncoupler present in all conditions, to ensure that activity was not inhibited by "back pressure" from PMF. Nearly all ATPase activity of WT and mutant membranes was likely due to F_0F_1 because sodium azide, a catalytic site inhibitor, reduced ATPase ≥98%. In direct comparison, ϵΔ5 and ϵ88stop membranes showed 63 and 60% ATPase activity *versus* WT (Table 2). However, when results were normalized for the F_0F_1 content in membranes, intrinsic ATPase activity was 2.6-fold higher in the complete absence of the ϵCTD (ϵ88stop). This is consistent with prior demonstrations that WT membrane ATPase activity doubled when ϵ inhibition was disrupted (12, 44). In contrast, the ϵΔ5 truncation did not significantly alter the intrinsic ATPase activity of F_0F_1 in membranes. This is also supported by the effects of LDAO, a detergent that is known to activate ATPase of *E. coli* F_0F_1 and F_1 mostly by disrupting ϵ inhibition (45, 46). LDAO activated ATPase activity to the same extent for WT and ϵΔ5 membranes but less for ϵ88stop membranes, which were already activated by the absence of the ϵCTD (Table 1). These results suggest that the loss of ϵ's 5 C-terminal residues does not significantly alter the inherent energetic balance between active and ϵ-inhibited forms of F_0F_1 in membranes.

As suggested previously for ϵ88stop (22), it is possible that partial functional uncoupling of F_1 from F_0 contributes to the *in vivo* phenotypic defect of ϵΔ5. One result of this could be that some ATPase activity is not thermodynamically linked to PMF; under respiratory conditions that would drive net ATP synthesis through well coupled F_0F_1, unregulated ATP hydrolysis

TABLE 2

Effects of ϵCTD truncations on the *in vitro* activities of membranes

The values with ranges are means ±S.E. with the number of independent experiments for each assay noted in parentheses.

	ATP hydrolysis					Proton-pumping assays[f]	
ϵ	Specific activity[a]	Relative[b]	Stimulation by LDAO[c]	Inhibition by DCCD[d]	ATP synthesis[e]	Driven by NADH	Driven by ATP
				%		%	
WT	5.2 ± 0.3 (7)	1.0	1.9 ± 0.3 (7)	77 ±2 (5)	105 ± 7 (8)	71 ±2.8 (7)	64 ±2.6 (8)
ϵΔ5	3.3 ± 0.3 (9)	1.1	2.1 ± 0.1 (9)	73 ±2 (5)	38 ± 2 (5)	77 ±3.7 (3)	60 ±5.4 (4)
ϵ88stop	3.1 ± 0.6 (3)	2.6	1.4 ± 0.04 (3)	81 ±3 (3)	100 ± 8 (4)	59 ±1.7 (4)[g]	53 ±6.5 (4)[h]

[a] The units are μmol/min/mg of membrane protein. Each experiment included duplicate assays for each sample in each condition tested.
[b] ATPase normalized to levels of catalytic β subunit in membranes, relative to WT.
[c] Ratio of activity ± 0.5% LDAO in assay.
[d] Inhibition (%) after preincubation of membranes with DCCD (0.1 mM, 30 min, 4 °C); ϵΔ5 value is not significantly less than others (unpaired *t* tests, $p > 0.11$).
[e] The units are nmol ATP/min/mg of membrane protein.
[f] Maximal quenching (%) of ACMA fluorescence after addition of NADH (0.5 mM) or ATP (1 mM).
[g] Significantly different from WT or ϵΔ5 result (unpaired *t* tests, $p < 0.026$).
[h] Not significantly different from WT or ϵΔ5 result (unpaired *t* tests, $p \geq 0.18$).

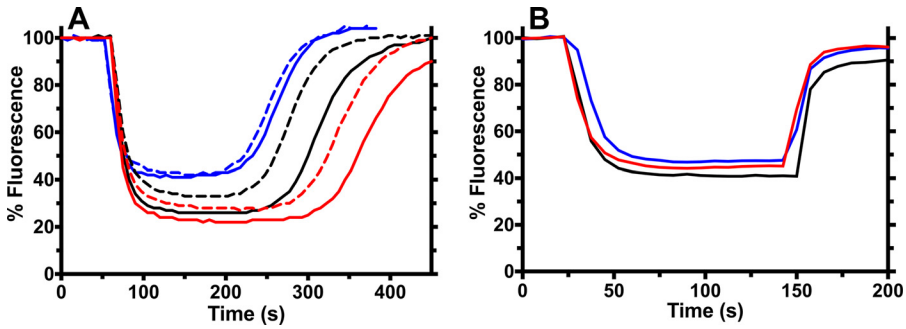

FIGURE 3. **Respiratory generation of proton motive force by membranes.** Proton pumping was measured by quenching of fluorescence of the dye ACMA (see "Experimental Procedures"). *A*, respiration was initiated by addition of NADH to 0.5 mM. *Dashed lines* represent proton pumping by untreated ϵ88stop (*blue*), ϵΔ5 (*red*), and WT (*black*) membranes. *Solid lines* represent proton pumping by the same membranes after treatment with DCCD to block possible proton leakage through F_0. Once the NADH was depleted, the relaxation of ACMA fluorescence quenching reflects all intrinsic membrane transport processes that contributed to collapse of the ΔpH. *B*, ATP was added to 1 mM to initiate proton pumping by F_0F_1, and after ~150 s, FCCP was added to 5 μM to collapse the PMF. Table 2 summarizes statistical results from multiple experiments for both NADH- and ATP-driven pumping.

would create a futile cycle that reduces the efficiency of cellular energy conversion. To test for this, ATP hydrolysis was measured after treating membranes with DCCD, a covalent modifier of the *c*-ring that blocks proton transport through F_0. For well coupled F_0F_1 complexes, blocking proton transport with DCCD also inhibits ATP hydrolysis (47). As shown in Table 2, the ϵ88stop truncation did not significantly alter the sensitivity of membrane ATPase to DCCD, although the original study by Cipriano and Dunn (22) showed slightly reduced DCCD inhibition for ϵ88stop membranes. The ϵΔ5 truncation resulted in a small and insignificant decrease in inhibition by DCCD (Table 2).

Membranes were also tested for possible effects of ϵCTD truncations on ATP synthesis. As shown in Table 2, ϵΔ5 membranes showed a >2.7-fold lower rate for ATP synthesis. This was not due to reduced PMF, because NADH-driven respiration generated similar ΔpH gradients for WT and ϵΔ5 membranes (Fig. 3 and Table 2). The lower ATP synthesis rate was also not due to the ~50% lower F_0F_1 content in ϵΔ5 membranes because ϵ88stop membranes had even lower F_0F_1 content (Table 1) but had ATP synthesis rates similar to that of WT pAU1 membranes (Table 2). This is consistent with prior studies showing that F_0F_1 content of haploid membranes exceeds that necessary for ATP synthesis rates *in vivo* (48) and *in vitro* (49). In fact, because ϵΔ5 membranes had more F_0F_1 than ϵ88stop or WT haploid membranes, their 2.7-fold lower synthesis rate probably reflects an even greater intrinsic inhibition of ATP synthesis by the ϵΔ5 subunit. Control assays were also included to test whether reduced ATP synthesis by ϵΔ5 membranes was due in part to any uncoupled ATPase activity. The ATP synthesis rates of ϵΔ5 and WT membranes were not significantly altered by the presence of 10 μM AMPPNP, which inhibits ATPase but not ATP synthesis (50). Together, these results indicate that the ϵΔ5 truncation directly increases ϵ inhibition of ATP synthesis by F_0F_1.

Another test for possible coupling defects between F_1 and F_0 is to monitor the kinetics of proton pumping by isolated, inverted membranes. Altered coupling between F_1 and F_0 might allow uncontrolled, passive flux of protons, which would decrease the capacity to generate PMF by respiration or by ATPase-driven proton pumping (51). As shown in Table 2 and Fig. 3*A* for NADH-driven proton pumping, ϵΔ5 membranes generated similar or better PMF than did WT, but ϵ88stop membranes generated partially reduced PMF. To test for F_0-specific proton leaks, membranes were treated with DCCD before addition of NADH. DCCD had a similar effect on NADH-driven proton pumping for WT and ϵΔ5 membranes (Fig. 3), so ϵΔ5 did not cause any increased leak through F_0. Fig. 3 also shows that the lower PMF achieved with ϵ88stop membranes (Table 2) was not due to greater proton leaks, because (i) upon depletion of NADH, the gradient collapsed with a time course similar to WT and ϵΔ5 membranes, and (ii) DCCD had a minimal effect on proton pumping by ϵ88stop membranes. The reduced PMF generated with ϵ88stop membranes was not

TABLE 3

Apparent F_1/ϵ dissociation rates for conditions shown in Fig. 4

Dissociation parameters are given for the nonlinear regression lines shown in Fig. 4. For the top four sample rows, all parameter values have standard errors <2%, and fits have R^2 values > 0.996. For the bottom two rows, insufficient dissociation occurred for reliable fitting; 10^{-6} s^{-1} is the slowest rate that can be fit reliably under the experimental conditions.

Conditions for association	Conditions for dissociation	ϵ (Fig. 4 trace)	Amplitude 1	k_{d1}	Amplitude 2	k_{d2}
			% total	s^{-1}	*% total*	s^{-1}
Buffer	Buffer	ϵ88stop (trace 6)	96	3.0×10^{-3}	1.3	$<10^{-6}$
Buffer	Buffer	ϵΔ5 (trace 1)	87	1.6×10^{-5}	12	9.5×10^{-4}
Buffer	ATP-EDTA	ϵΔ5 (trace 2)	94	6.3×10^{-4}	6	2.9×10^{-3}
Buffer	ATP-EDTA	WT-ϵ (trace 3)	94	4.0×10^{-3}	5	$<10^{-6}$
ATP-EDTA	MgADP-Pi	WT-ϵ (trace 4)	~100	$<10^{-6}$		
ATP-EDTA	MgADP-Pi	ϵΔ5 (trace 5)	~100	$<10^{-6}$		

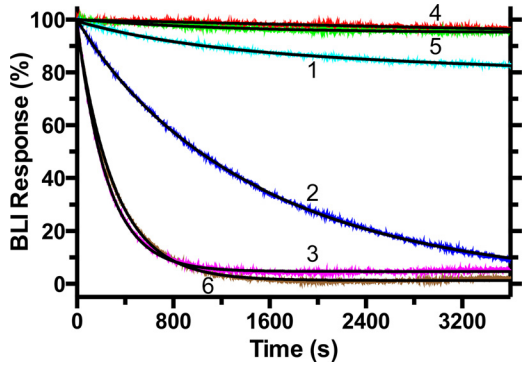

FIGURE 4. **Effects of ϵΔ5 on dissociation of F_1/ϵ complexes.** Only the dissociation phase is shown for representative BLI assays. In previous steps, similar amounts of biotinylated ϵ (Bap-ϵ, WT, ϵ88stop, or ϵΔ5) were immobilized on streptavidin-coated BLI sensors, and then sensors were incubated 15 min with excess F_1(-δε) to form F_1/ϵ complexes (100% BLI signal, nm: *trace 1*, 0.51; *traces 2–5*, done in parallel, 0.39 ± 0.02; *trace 6*, 0.6). Buffer conditions for association/dissociation phases: *trace 1* (ϵΔ5, *cyan*) and *trace 6* (ϵ88stop, *brown*), buffer/buffer; *trace 2* (ϵΔ5, *blue*) and *trace 3* (WT-ϵ, *magenta*), buffer/ATP-EDTA (1 mM each); *trace 4* (WT-ϵ, *red*) and *trace 5* (ϵΔ5, *green*), 1 mM ATP-EDTA/(2 mM Mg^{2+}, 1 mM ADP, 1 mM Pi). *Black lines* are nonlinear regression fits (GraphPad Prism) for two phases of exponential decay; fitting results are summarized in Table 3. Note that data for *trace 6* are reproduced from Ref. 15.

due to gross changes in the capacity of the electron transport chain, because two preparations of ϵ88stop membranes showed NADH oxidation rates at least as fast as with WT membranes (0.8 and 0.7 μmol/min/mg protein, respectively).[4] In any case, the current proton pumping results show that the ϵCTD truncations do not cause any increased proton leak in the membrane preparations. Proton pumping was also tested when PMF was generated by ATP hydrolysis via F_0F_1, and results were similar for WT, ϵΔ5, and ϵ88stop membranes (Table 2 and Fig. 3*B*). Cipriano and Dunn (22) noted a more significant defect in ATPase-driven proton pumping for ϵ88stop; there is no apparent reason for this discrepancy, although different host strains of *E. coli* were used.

Effects of ϵΔ5 Truncation on Interactions of ϵCTD with Isolated F_1—In vitro, the catalytic complex of ATP synthases can be released from the membrane as a soluble F_1-ATPase. Isolated bacterial F_1 is strongly inhibited by ϵ but, upon dilution, ϵ can dissociate, activating the enzyme (2, 9). Previously, BLI kinetic assays of protein-protein interactions showed that the conformation of the ϵCTD controls dissociation of ϵ from *E. coli* F_1 (15), and ϵ probably does not dissociate at all when it adopts the inhibitory extended conformation (ϵ_X), with part of the ϵCTD buried in the central cavity of F_1 (13, 15). Here, BLI was used to test whether the ϵΔ5 truncation changes the interactions of ϵCTD with F_1. With F_1 bound to immobilized ϵΔ5 in buffer alone, 87% of F_1/ϵΔ5 complexes dissociated very slowly in buffer only (Fig. 4, *trace 1*, and Table 3). This is similar to the behavior of F_1/WT-ϵ (15), but the difference in their slow dissociation rates is near the limit of sensitivity for BLI in these conditions. Although WT-ϵ on F_1 is strongly biased toward the tightly bound inhibitory state, transition in and out of that state is dynamic (14, 15); addition of excess ATP in the BLI dissociation step (with EDTA present to prevent hydrolysis) rapidly shifts F_1/WT-ϵ complexes to dissociate ~80-fold faster, as if the ϵCTD were completely absent (Fig. 4, *traces 3* and *6*). ATP/EDTA in the dissociation step produced faster, essentially monophasic dissociation of F_1/ϵΔ5 complexes (Fig. 4, *trace 2*) with no noticeable lag, but with a rate ~6-fold slower than for F_1/WT-ϵ (Table 3). As seen before (15), when F_1/WT-ϵ was bound in the presence of ATP/EDTA, subsequent exposure to Mg^{2+} allowed hydrolysis and rapid switching to the ϵ-inhibited state at the catalytic dwell, and post-hydrolysis conditions (MgADP/Pi) in the dissociation step stabilized ϵ in the tightly bound form (Fig. 4, *trace 4*). F_1/ϵΔ5 complexes also showed rapid reversal to a tightly bound state on switching from ATP/EDTA during F_1/ϵΔ5 association to MgADP/P_i in the dissociation phase (Fig. 4, *trace 5*). Overall, these results indicate that although the ϵCTD can still undergo dynamic transitions between different conformations, the absence of five terminal residues from the ϵCTD significantly stabilizes a tightly bound state of ϵΔ5 on F_1 relative to the dissociable state.

The ATPase activity of isolated *E. coli* F_1 is inhibited >90% by bound WT-ϵ (9, 15). Because ϵΔ5 showed a bias toward tight binding, we investigated whether this correlates with greater inhibition. An N-terminal Bap tag on ϵ does not affect its inhibition of isolated F_1 (15). As shown in Fig. 5, the K_I of 0.7 nM for Bap-ϵΔ5 is similar to the K_I for WT-ϵ (0.5 nM) but does not reflect the increased stability of the tightly bound state as indicated by the BLI assays of F_1/ϵΔ5 binding. Furthermore, maximal inhibition by ϵΔ5 was only ~20%. This is similar to the ~24% maximal inhibition by ϵ88stop under the same conditions, although the K_I for ϵ88stop is nearly 20-fold weaker because of the complete absence of the ϵCTD (15). This surprising finding indicates that the shorter ϵCTD of ϵΔ5 still con-

[4] *E. coli* expresses two types of NADH dehydrogenase, only one of which pumps protons, and expresses different terminal oxidases with different contributions to generating PMF (75). Thus, the reduced PMF could occur if the ϵ88stop membranes predominantly expressed the less efficient respiratory complexes. Changes in expression of these respiratory complexes have been noted to occur in response to an ATP synthase mutant (76).

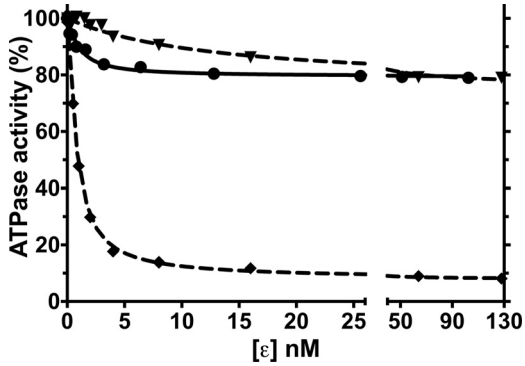

FIGURE 5. **Inhibition of F_1-ATPase by WT and truncated forms of the ϵ subunit.** Results for WT-ϵ (◆) and ϵ88stop (▼) are reproduced from (15). Assays with varied concentrations of ϵΔ5 subunit (●) were measured with 0.75 nM F_1(-δϵ). The specific activity of F_1(-δϵ) alone was 60.9 μmol/min/mg. For each data set, the curve shown is from a nonlinear regression fit to a quadratic equation described in Ref. 15. For ϵΔ5, regression indicated maximal inhibition of F_1(-δϵ) = 20% (95% confidence interval, 19–22%), and K_I = 0.68 nM (95% confidence interval, 0.33–1.02 nM); R^2 = 0.972 (GraphPad Prism). In parallel with ϵΔ5 assays, control assays confirmed that 100 nM WT-ϵ inhibited F_1(-δϵ) >85%.

tributes to tight binding to F_1, but that the five terminal residues of ϵ are critical for strong inhibition of F_1-ATPase activity. However, ϵΔ5 does inhibit ATP synthesis and hydrolysis by F_0F_1 on membranes (Table 2), suggesting that F_0-F_1 interactions are important for the ϵΔ5 subunit to achieve inhibition of ATP hydrolysis.

Discussion

Earlier studies with F_0F_1 of *E. coli* (52) and *B. PS3* (53) suggested that the extended ϵCTD inhibits ATPase but not ATP synthesis, based on disulfide cross-links to trap the ϵCTD in extended states. However, it is not clear that those γ–ϵ cross-links occurred in native conformations of the enzyme. For example, the *E. coli* cross-linking sites (γ99, ϵ118) were based on a structure of an isolated complex of truncated γ with ϵ (54), but are 28 Å apart (Cα-Cα) in the structure determined for ϵ-inhibited F_1 (13). Subsequent studies showed that deleting the ϵCTD increased the ATP synthesis rate 3-fold for *B. PS3* F_0F_1 (10) and activated ATP synthesis more than it activated ATPase for *E. coli* F_0F_1, (11). Thus, it is clear that the ϵCTD can inhibit both ATP hydrolytic and synthetic directions of rotary catalysis in bacterial ATP synthases. Here, *in vitro* results for F_0F_1 containing the ϵΔ5 subunit further show that altering interactions of the ϵCTD with F_1 can preferentially increase inhibition of ATP synthesis (Table 2).

Prior studies with membrane-bound *E. coli* F_0F_1 (12, 44) indicate that, on average, ~50% of F_0F_1 complexes are in an ϵ-inhibited state. Current results with ϵ88stop membranes support this, because the intrinsic ATPase activity is 2.6-fold greater in the absence of the ϵCTD (relative ATP hydrolysis in Table 2). ATP synthesis results with ϵ88stop membranes also likely reflect a greater fraction of active F_0F_1 complexes without the ϵCTD: compared with WT, ϵ88stop membranes showed about the same synthesis rates (Table 2), although they contained ~4-fold less F_0F_1 (Table 1) and generated lower PMF by NADH oxidation (Fig. 3). In the presence of MgADP/Pi, PMF activates F_0F_1 in *E. coli* membranes (55), probably because of release from the ϵ-inhibited state (13, 15). Thus, without the inhibitory ϵCTD, ϵ88stop membranes in this study likely contained a higher fraction of active F_0F_1 complexes and so achieved high ATP synthesis rates even with a reduced PMF. In contrast, ϵΔ5 membranes showed ATP synthesis rates nearly 3-fold less than those for WT or ϵ88stop (Table 2), even though F_0F_1 content was ~2-fold greater in ϵΔ5 than in ϵ88stop membranes (Table 1). The low synthesis rate was not due to uncoupling, because ϵΔ5 membranes generated a greater NADH-driven pH gradient than did WT and showed no greater F_0-specific proton leak (Fig. 3). On the other hand, ϵΔ5 membranes showed intrinsic ATPase rates, activation by LDAO, and ATPase-driven proton pumping that were very similar to the values obtained with WT membranes (Table 2). Thus, the ϵΔ5 truncation specifically increased ϵ inhibition of ATP synthesis without increasing inhibition of ATP hydrolysis or uncoupling ATPase from proton pumping. Further, without interactions with F_0, ϵΔ5 subunit bound isolated F_1 with high affinity (Fig. 4) but inhibited F_1-ATPase minimally, as seen with the ϵNTD alone (Fig. 5). This suggests that contacts of the ϵ-hook with the CTD of subunit β3 (Fig. 1*B*) are important for inhibition of F_1-ATPase.

Differential effects on ATP synthesis *versus* hydrolysis modes have been noted for other inhibitors (reviewed in Ref. 50). For example, azide or AMPPNP inhibit ATP hydrolysis but not ATP synthesis, whereas some fluorescent analogs of ADP inhibit ATP synthesis more than hydrolysis. However, what mechanisms might explain how the ϵΔ5 truncation selectively increases inhibition of ATP synthesis? Thus far, only one ϵ-inhibited state has been observed structurally (13). If one assumes that the observed ϵ_X state is responsible for inhibition of both synthesis and hydrolysis, then the ϵΔ5 truncation could preferentially increase the energy barrier for activation from the ϵ_X state during rotation in the direction of ATP synthesis. Control of ϵ conformation by rotational direction has been proposed before (56). Such directional asymmetry has been demonstrated for an ADP-inhibited state that pauses the enzyme at a specific rotary angle: in single-molecule studies with *B. PS3* F_1, magnetically driven torque reactivated the enzyme after 40° of forced rotation in the direction of hydrolysis but not after 120° in the direction of ATP synthesis (57). For regulation by the ϵCTD, an alternative is the bidirectional ratchet model, in which the ϵCTD has distinct regulatory interactions with F_1 during opposite directions of rotary catalysis (6, 58). With this model, the ϵΔ5 truncation could preferentially enhance the stability of the inhibitory state that forms primarily during ATP synthesis mode. Our present results on interactions of the ϵΔ5 subunit with isolated F_1 seem more consistent with this second model: kinetic assays for F_1/ϵ interactions (Fig. 4) indicate that the tightly bound state of F_1/ϵΔ5 reverses to a dissociable state more slowly than for F_1/WT-ϵ, but the tightly bound state of ϵΔ5 causes minimal inhibition of F_1-ATPase activity (Fig. 5).

The existence of a distinct F_1/ϵCTD interaction state is also consistent with our recent collaborations to study conformational changes of the ϵCTD by single-molecule FRET with probes on γ and on helix-1 of the ϵCTD. Initial studies with isolated F_1 (59, 60) showed bimodal distribution of FRET efficiencies that correlate with the ϵ_C and ϵ_X states, and nucleotides shifted the balance between the two FRET states in agreement

with our bulk assays of F_1/ϵ interactions (15). Subsequent studies with FRET-labeled F_0F_1-liposomes revealed a trimodal distribution of FRET efficiencies in the presence of MgATP that cannot be explained by the two known orientations of helix-1 of ϵ (13, 16). Thus, it seems likely that the ϵCTD can form distinct interactions with F_1 during opposite directions of rotary catalysis and that ϵΔ5 preferentially stabilizes or promotes formation of the tightly bound state that inhibits the ATP synthesis direction.

For the direction of ATP hydrolysis, single-molecule rotation assays (14, 61, 62) and our recent enzymological study (15) show that inhibition by the ϵCTD initiates at the catalytic dwell angle after the hydrolytic step. In contrast, the only available structure of ϵ-inhibited F_1 appears to be paused after further 40° rotation to an angle near the next dwell for ATP binding (13). Some rotational data could suggest dynamic oscillation between these two angles during a long inhibitory pause (Ref. 14 and Fig. 3*A*), so perhaps these represent two positions of the ϵCTD that have distinct regulatory effects during opposite directions of rotary catalysis. In detail, ϵΔ5 might also cause some type of mechanical slip between F_1 and F_0 only during rotation in the ATP synthesis direction, but further tests are needed to explore these possibilities.

Correlation of the ϵΔ5 Phenotypic Growth Defect with Inhibited ATP Synthesis—Reduced ATP synthesis rate was the only significant functional defect identified *in vitro* with ϵΔ5 membranes, and this is likely the primary reason that cells expressing ϵΔ5 grew poorly by oxidative phosphorylation. With the entire ϵCTD absent, cells showed better phenotypic growth, and rates of *in vitro* ATP synthesis were normal, even though ϵ88stop membranes contained less F_0F_1. An earlier study reported that deletion of 10 C-terminal residues from *E. coli* ϵ also allowed normal growth yield on succinate (23), indicating that *in vivo* ATP synthesis is more effective than with ϵΔ5. Together, these results suggest that residues between ϵ128–133 are important for inhibition of ATP synthesis.

It should be noted that the pAU1 construct used here expresses the entire *atp* operon, and ϵΔ5 membranes contained ~4-fold greater F_0F_1 than in haploid membranes. Even haploid expression of *E. coli* F_0F_1 is not rate-limiting for ATP synthesis *in vivo* (48), so the low rate measured for *in vitro* ATP synthesis by ϵΔ5 membranes probably represents a greater intrinsic inhibition by ϵΔ5. Thus, ϵΔ5 should cause an even larger defect in phenotypic growth in a strain expressing lower, haploid levels of F_0F_1, and we are currently reengineering our expression system to test for this.

Summary—Overall, our results are consistent with the idea that the ϵCTD may be fine-tuned in different bacterial species to regulate ATP synthesis and hydrolysis functions according to the distinct metabolic/environmental demands of each species (2, 9). We showed that a minor truncation of the ϵ-hook selectively increased inhibition of ATP synthesis and reduced the capacity for cell growth on a nonfermentable carbon source. ATP synthases from two Gram-positive species appear to be missing the last 3–4 residues of the ϵ hook (17, 18) but still show strong inhibition of ATPase by ϵ (20, 21). This could suggest that inhibitory behavior in different species involves co-evolution of one or more subunits that interact with the ϵCTD. This correlates with results of recent computational studies of co-evolution in protein complexes, which used interactions of γ and ϵ as a test case (63, 64). There are also indications that ϵ inhibition also occurs in the enzyme of several species of *Mycobacterium* (65, 66), and the CTD of most mycobacterial ϵ subunits is ~17 residues shorter than that of *E. coli*, although different possible alignments make it uncertain how much of the hook and/or helix-2 are absent (67, 68). Mycobacterial ATP synthase is the target of a new class of antibiotics, the diarylquinolines, and the lead drug, bedaquiline, has been approved for treatment of multidrug-resistant tuberculosis (25, 69). Modified diarylquinolines have been developed to attack other Gram-positive pathogens including *Staphylococcus aureus* but so far, these show significant inhibition of mitochondrial ATP synthase (70). Bacterial ATP synthase function is also essential or important for the viability or virulence of Gram-negative pathogens (71–74). Thus, it will be important to explore how ϵ inhibits ATP synthases in a range of bacterial pathogens. Results of the current study support the concept that ϵ inhibition can provide a bacteria-specific means to target the ATP synthase for development of future antibiotics.

Author Contributions—N. B. S. performed all experiments shown. T. M. D. prepared Fig. 1. N. B. S. and T. M. D. conceived the study, wrote the paper, analyzed and reviewed all results, and approved the final version of the manuscript.

Acknowledgments—We thank Nancy Walker-Kopp for technical assistance with immunoblotting. We thank Prof. Alan Senior (University of Rochester Medical Center, Rochester, NY) for the gift of the βM209L mutant.

References

1. Boyer, P. D. (1997) The ATP synthase: a splendid molecular machine. *Annu. Rev. Biochem.* **66,** 717–749
2. Duncan, T. M. (2004) The ATP synthase: parts and properties of a rotary motor. In *The Enzymes*, Vol. XXIII: Energy Coupling and Molecular Motors (Hackney, D. D., and Tamanoi, F., eds) 3rd Ed., pp. 203–275, Elsevier Academic Press, New York
3. von Ballmoos, C., Cook, G. M., and Dimroth, P. (2008) Unique rotary ATP synthase and its biological diversity. *Annu. Rev. Biophys.* **37,** 43–64
4. Junge, W., and Nelson, N. (2015) ATP synthase. *Annu. Rev. Biochem.* **84,** 631–657
5. Cox, G. B., Devenish, R. J., Gibson, F., Howitt, S. M., and Nagley, P. (1992) The structure and assembly of ATP synthase. In *Molecular Mechanisms in Bioenergetics* (Ernster, L., ed) pp. 283–315, Elsevier Science, New York
6. Dunn, S. D., Cipriano, D. J., and Del Rizzo, P. A. (2004) ATP synthase stalk subunits *b*, ™ and Σ: structures and functions in energy coupling. In *Handbook of ATPases* (Futai, M., Wada, Y., and Kaplan, J. H., eds) pp. 311–338, Wiley-VCH Verlag, Weinheim, Germany
7. Harris, D. A., and Das, A. M. (1991) Control of mitochondrial ATP synthesis in the heart. *Biochem. J.* **280,** 561–573
8. Walker, J. E. (1994) The regulation of catalysis in ATP synthase. *Curr. Opin. Struct. Biol.* **4,** 912–918
9. Feniouk, B. A., Suzuki, T., and Yoshida, M. (2006) The role of subunit ϵ in the catalysis and regulation of F_0F_1-ATP synthase. *Biochim. Biophys. Acta* **1757,** 326–338
10. Masaike, T., Suzuki, T., Tsunoda, S. P., Konno, H., and Yoshida, M. (2006) Probing conformations of the β subunit of F_0F_1-ATP synthase in catalysis. *Biochem. Biophys. Res. Commun.* **342,** 800–807
11. Iino, R., Hasegawa, R., Tabata, K. V., and Noji, H. (2009) Mechanism of inhibition by C-terminal α-helices of the ϵ subunit of *Escherichia coli*

F_0F_1-ATP synthase. *J. Biol. Chem.* **284,** 17457–17464
12. Schulenberg, B., and Capaldi, R. A. (1999) The ϵ subunit of the F_1F_0 complex of *Escherichia coli*: cross-linking studies show the same structure *in situ* as when isolated. *J. Biol. Chem.* **274,** 28351–28355
13. Cingolani, G., and Duncan, T. M. (2011) Structure of the ATP synthase catalytic complex (F_1) from *Escherichia coli* in an autoinhibited conformation. *Nat. Struct. Mol. Biol.* **18,** 701–707
14. Sekiya, M., Hosokawa, H., Nakanishi-Matsui, M., Al-Shawi, M. K., Nakamoto, R. K., and Futai, M. (2010) Single molecule behavior of inhibited and active states of *Escherichia coli* ATP synthase F_1 rotation. *J. Biol. Chem.* **285,** 42058–42067
15. Shah, N. B., Hutcheon, M. L., Haarer, B. K., and Duncan, T. M. (2013) F_1-ATPase of *Escherichia coli*: the ϵ-inhibited state forms after ATP hydrolysis, is distinct from the ADP-inhibited state, and responds dynamically to catalytic-site ligands. *J. Biol. Chem.* **288,** 9383–9395
16. Wilkens, S., and Capaldi, R. A. (1998) Solution structure of the ϵ subunit of the F_1-ATPase from *Escherichia coli* and interactions of this subunit with β subunits in the complex. *J. Biol. Chem.* **273,** 26645–26651
17. Yagi, H., Kajiwara, N., Tanaka, H., Tsukihara, T., Kato-Yamada, Y., Yoshida, M., and Akutsu, H. (2007) Structures of the thermophilic F_1-ATPase ϵ subunit suggesting ATP-regulated arm motion of its C-terminal domain in F_1. *Proc. Natl. Acad. Sci. U.S.A.* **104,** 11233–11238
18. Stocker, A., Keis, S., Vonck, J., Cook, G. M., and Dimroth, P. (2007) The structural basis for unidirectional rotation of thermoalkaliphilic F_1-ATPase. *Structure* **15,** 904–914
19. Gibbons, C., Montgomery, M. G., Leslie, A. G., and Walker, J. E. (2000) The structure of the central stalk in bovine F_1-ATPase at 2.4 Å resolution. *Nat. Struct. Biol.* **7,** 1055–1061
20. Kato-Yamada, Y., Bald, D., Koike, M., Motohashi, K., Hisabori, T., and Yoshida, M. (1999) ϵ subunit, an endogenous inhibitor of bacterial F_1-ATPase, also inhibits F_0F_1-ATPase. *J. Biol. Chem.* **274,** 33991–33994
21. Keis, S., Stocker, A., Dimroth, P., and Cook, G. M. (2006) Inhibition of ATP hydrolysis by thermoalkaliphilic F_1F_o-ATP synthase is controlled by the C terminus of the ϵ subunit. *J. Bacteriol.* **188,** 3796–3804
22. Cipriano, D. J., and Dunn, S. D. (2006) The role of the ϵ subunit in the *Escherichia coli* ATP synthase: the C-terminal domain is required for efficient energy coupling. *J. Biol. Chem.* **281,** 501–507
23. Kuki, M., Noumi, T., Maeda, M., Amemura, A., and Futai, M. (1988) Functional domains of ϵ subunit of *Escherichia coli* H^+-ATPase (F_0F_1). *J. Biol. Chem.* **263,** 17437–17442
24. Jounouchi, M., Takeyama, M., Noumi, T., Moriyama, Y., Maeda, M., and Futai, M. (1992) Role of the amino terminal region of the ϵ subunit of *Escherichia coli* H^+-ATPase (F_0F_1). *Arch. Biochem. Biophys.* **292,** 87–94
25. Andries, K., Verhasselt, P., Guillemont, J., Göhlmann, H. W., Neefs, J. M., Winkler, H., Van Gestel, J., Timmerman, P., Zhu, M., Lee, E., Williams, P., de Chaffoy, D., Huitric, E., Hoffner, S., Cambau, E., Truffot-Pernot, C., Lounis, N., and Jarlier, V. (2005) A diarylquinoline drug active on the ATP synthase of *Mycobacterium tuberculosis*. *Science* **307,** 223–227
26. Duncan, T. M., Zhou, Y., Bulygin, V. V., Hutcheon, M. L., and Cross, R. L. (1995) Probing interactions of the *Escherichia coli* F_0F_1 ATP synthase β and γ subunits with disulphide cross-links. *Biochem. Soc. Trans.* **23,** 736–741
27. Braman, J., Papworth, C., and Greener, A. (1996) Site-directed mutagenesis using double-stranded plasmid DNA templates. *Methods Mol. Biol.* **57,** 31–44
28. Wilke-Mounts, S., Pagan, J., and Senior, A. E. (1995) Mutagenesis and reversion analysis of residue Met-209 of the β-subunit of *Escherichia coli* ATP synthase. *Arch. Biochem. Biophys.* **324,** 153–158
29. Schaefer, E. M., Hartz, D., Gold, L., and Simoni, R. D. (1989) Ribosome-binding sites and RNA-processing sites in the transcript of the *Escherichia coli unc* operon. *J. Bacteriol.* **171,** 3901–3908
30. Gibson, F., Cox, G. B., Downie, J. A., and Radik, J. (1977) Partial diploids of *Escherichia coli* carrying normal and mutant alleles affecting oxidative phosphorylation. *Biochem. J.* **162,** 665–670
31. Klionsky, D. J., Brusilow, W. S., and Simoni, R. D. (1984) *In vivo* evidence for the role of the ϵ subunit as an inhibitor of the proton-translocating ATPase of *Escherichia coli*. *J. Bacteriol.* **160,** 1055–1060
32. Wise, J. G. (1990) Site-directed mutagenesis of the conserved β subunit tyrosine 331 of *Escherichia coli* ATP synthase yields catalytically active enzymes. *J. Biol. Chem.* **265,** 10403–10409
33. Grant, S. G., Jessee, J., Bloom, F. R., and Hanahan, D. (1990) Differential plasmid rescue from transgenic mouse DNAs into *Escherichia coli* methylation-restriction mutants. *Proc. Natl. Acad. Sci. U.S.A.* **87,** 4645–4649
34. Peterson, G. L. (1977) A simplification of the protein assay method of Lowry *et al*. which is more generally applicable. *Anal. Biochem.* **83,** 346–356
35. Laemmli, U. K. (1970) Cleavage of structural proteins during the assembly of the head of bacteriophage T4. *Nature* **227,** 680–685
36. Mnatsakanyan, N., Krishnakumar, A. M., Suzuki, T., and Weber, J. (2009) The role of the βDELSEED-loop of ATP synthase. *J. Biol. Chem.* **284,** 11336–11345
37. Pullman, M. E., Penefsky, H. S., Datta, A., and Racker, E. (1960) Partial resolution of the enzymes catalysing oxidative phosphorylation: I. purification and properties of soluble dinitrophenyl-stimulated adonosine triphophatase. *J. Biol. Chem.* **235,** 3322–3329
38. Tomashek, J. J., Glagoleva, O. B., and Brusilow, W. S. (2004) The *Escherichia coli* F_1F_0 ATP synthase displays biphasic synthesis kinetics. *J. Biol. Chem.* **279,** 4465–4470
39. Vik, S. B., Cain, B. D., Chun, K. T., and Simoni, R. D. (1988) Mutagenesis of the a subunit of the F_1F_0-ATPase from *Escherichia coli*: mutations at Glu-196, Pro-190, and Ser-199. *J. Biol. Chem.* **263,** 6599–6605
40. Shah, N. B., and Duncan, T. M. (2014) Bio-layer interferometry for measuring kinetics of protein-protein interactions and allosteric ligand effects. *J. Vis. Exp.* **84,** e51383
41. Gibson, F. (2000) The introduction of *Escherichia coli* and biochemical genetics to the study of oxidative phosphorylation. *Trends Biochem. Sci.* **25,** 342–344
42. Duncan, T. M., and Senior, A. E. (1985) The defective proton-ATPase of *uncD* mutants of *Escherichia coli*: two mutations which affect the catalytic mechanism. *J. Biol. Chem.* **260,** 4901–4907
43. Boogerd, F. C., Boe, L., Michelsen, O., and Jensen, P. R. (1998) ATP mutants of *Escherichia coli* fail to grow on succinate due to a transport deficiency. *J. Bacteriol.* **180,** 5855–5859
44. Mendel-Hartvig, J., and Capaldi, R. A. (1991) Nucleotide-dependent and dicyclohexylcarbodiimide-sensitive conformational changes in the ϵ subunit of *Escherichia coli* ATP synthase. *Biochemistry* **30,** 10987–10991
45. Lötscher, H. R., deJong, C., and Capaldi, R. A. (1984) Interconversion of high and low adenosinetriphosphatase activity forms of *Escherichia coli* F_1 by the detergent lauryldimethylamine oxide. *Biochemistry* **23,** 4140–4143
46. Dunn, S. D., Tozer, R. G., and Zadorozny, V. D. (1990) Activation of *Escherichia coli* F_1-ATPase by lauryldimethylamine oxide and ethylene glycol: relationship of ATPase activity to the interaction of the ϵ and β subunits. *Biochemistry* **29,** 4335–4340
47. Hermolin, J., and Fillingame, R. H. (1989) H_+-ATPase activity of *Escherichia coli* F_1F_0 is blocked after reaction of dicyclohexylcarbodiimide with a single proteolipid (subunit c) of the F_0 complex. *J. Biol. Chem.* **264,** 3896–3903
48. Jensen, P. R., Westerhoff, H. V., and Michelsen, O. (1993) Excess capacity of H^+-ATPase and inverse respiratory control in *Escherichia coli*. *EMBO J.* **12,** 1277–1282
49. Etzold, C., Deckers-Hebestreit, G., and Altendorf, K. (1997) Turnover number of *Escherichia coli* F_0F_1 ATP synthase for ATP synthesis in membrane vesicles. *Eur. J. Biochem.* **243,** 336–343
50. Hong, S., and Pedersen, P. L. (2008) ATP synthase and the actions of inhibitors utilized to study its roles in human health, disease, and other scientific areas. *Microbiol. Mol. Biol. Rev.* **72,** 590–641
51. Zhang, Y., Oldenburg, M., and Fillingame, R. H. (1994) Suppressor mutations in F_1 subunit ϵ recouple ATP-driven H^+ translocation in uncoupled Q42E subunit c mutant of *Escherichia coli* F_1F_0 ATP synthase. *J. Biol. Chem.* **269,** 10221–10224
52. Tsunoda, S. P., Rodgers, A. J., Aggeler, R., Wilce, M. C., Yoshida, M., and Capaldi, R. A. (2001) Large conformational changes of the ϵ subunit in the bacterial F_1F_0 ATP synthase provide a ratchet action to regulate this rotary motor enzyme. *Proc. Natl. Acad. Sci. U.S.A.* **98,** 6560–6564
53. Suzuki, T., Murakami, T., Iino, R., Suzuki, J., Ono, S., Shirakihara, Y., and Yoshida, M. (2003) F_0F_1-ATPase/synthase is geared to the synthesis mode

by conformational rearrangement of ϵ subunit in response to proton motive force and ADP/ATP balance. *J. Biol. Chem.* **278,** 46840–46846
54. Rodgers, A. J., and Wilce, M. C. (2000) Structure of the γ-ϵ complex of ATP synthase. *Nat. Struct. Biol.* **7,** 1051–1054
55. Fischer, S., Graber, P., and Turina, P. (2000) The activity of the ATP synthase from *Escherichia coli* is regulated by the transmembrane proton motive force. *J. Biol. Chem.* **275,** 30157–30162
56. Feniouk, B. A., and Junge, W. (2005) Regulation of the F_0F_1-ATP synthase: the conformation of subunit ϵ might be determined by directionality of subunit γ rotation. *FEBS Lett.* **579,** 5114–5118
57. Hirono-Hara, Y., Ishizuka, K., Kinosita, K., Jr., Yoshida, M., and Noji, H. (2005) Activation of pausing F_1 motor by external force. *Proc. Natl. Acad. Sci. U.S.A.* **102,** 4288–4293
58. Cipriano, D. J., Bi, Y., and Dunn, S. D. (2002) Genetic fusions of globular proteins to the ϵ subunit of the *Escherichia coli* ATP synthase: implications for *in vivo* rotational catalysis and ϵ subunit function. *J. Biol. Chem.* **277,** 16782–16790
59. Börsch, M., and Duncan, T. M. (2013) Spotlighting motors and controls of single F_0F_1-ATP synthase. *Biochem. Soc. Trans.* **41,** 1219–1226
60. Bockenhauer, S. D., Duncan, T. M., Moerner, W. E., and Börsch, M. (2014) The regulatory switch of F_1-ATPase studied by single-molecule FRET in the ABEL Trap. *Proc. SPIE* **8950,** 89500H-89501–89500H-89514
61. Konno, H., Murakami-Fuse, T., Fujii, F., Koyama, F., Ueoka-Nakanishi, H., Pack, C. G., Kinjo, M., and Hisabori, T. (2006) The regulator of the F_1 motor: inhibition of rotation of cyanobacterial F_1-ATPase by the ϵ subunit. *EMBO J.* **25,** 4596–4604
62. Tsumuraya, M., Furuike, S., Adachi, K., Kinosita, K., Jr., and Yoshida, M. (2009) Effect of ϵ subunit on the rotation of thermophilic Bacillus F_1-ATPase. *FEBS Lett.* **583,** 1121–1126
63. Hopf, T. A., Schärfe, C. P., Rodrigues, J. P., Green, A. G., Kohlbacher, O., Sander, C., Bonvin, A. M., and Marks, D. S. (2014) Sequence co-evolution gives 3D contacts and structures of protein complexes. *eLife* **3,** e03430
64. Iserte, J., Simonetti, F. L., Zea, D. J., Teppa, E., and Marino-Buslje, C. (2015) I-COMS: Interprotein-COrrelated Mutations Server. *Nucleic Acids Res.* **43,** W320–W325
65. Higashi, T., Kalra, V. K., Lee, S. H., Bogin, E., and Brodie, A. F. (1975) Energy-transducing membrane-bound coupling factor-ATPase from *Mycobacterium phlei*: I. purification, homogeneity, and properties. *J. Biol. Chem.* **250,** 6541–6548
66. Haagsma, A. C., Driessen, N. N., Hahn, M. M., Lill, H., and Bald, D. (2010) ATP synthase in slow- and fast-growing mycobacteria is active in ATP synthesis and blocked in ATP hydrolysis direction. *FEMS Microbiol. Lett.* **313,** 68–74
67. Biukovic, G., Basak, S., Manimekalai, M. S., Rishikesan, S., Roessle, M., Dick, T., Rao, S. P., Hunke, C., and Grüber, G. (2013) Variations of subunit ϵ of the *Mycobacterium tuberculosis* F_1F_0 ATP synthase and a novel model for mechanism of action of the tuberculosis drug TMC207. *Antimicrob. Agents Chemother.* **57,** 168–176
68. Lu, P., Lill, H., and Bald, D. (2014) ATP synthase in mycobacteria: special features and implications for a function as drug target. *Biochim. Biophys. Acta* **1837,** 1208–1218
69. Cohen, J. (2013) Approval of novel TB drug celebrated—with restraint. *Science* **339,** 130
70. Balemans, W., Vranckx, L., Lounis, N., Pop, O., Guillemont, J., Vergauwen, K., Mol, S., Gilissen, R., Motte, M., Lançois, D., De Bolle, M., Bonroy, K., Lill, H., Andries, K., Bald, D., and Koul, A. (2012) Novel antibiotics targeting respiratory ATP synthesis in gram-positive pathogenic bacteria. *Antimicrob. Agents Chemother.* **56,** 4131–4139
71. Bijlsma, J. J., Lie-A-Ling, M., Nootenboom, I. C., Vandenbroucke-Grauls, C. M., and Kusters, J. G. (2000) Identification of loci essential for the growth of *Helicobacter pylori* under acidic conditions. *J. Infect. Dis.* **182,** 1566–1569
72. de Berardinis, V., Vallenet, D., Castelli, V., Besnard, M., Pinet, A., Cruaud, C., Samair, S., Lechaplais, C., Gyapay, G., Richez, C., Durot, M., Kreimeyer, A., Le Fèvre, F., Schächter, V., Pezo, V., Döring, V., Scarpelli, C., Médigue, C., Cohen, G. N., Marlière, P., Salanoubat, M., and Weissenbach, J. (2008) A complete collection of single-gene deletion mutants of *Acinetobacter baylyi* ADP1. *Mol. Syst. Biol.* **4,** 174
73. Liberati, N. T., Urbach, J. M., Miyata, S., Lee, D. G., Drenkard, E., Wu, G., Villanueva, J., Wei, T., and Ausubel, F. M. (2006) An ordered, nonredundant library of *Pseudomonas aeruginosa* strain PA14 transposon insertion mutants. *Proc. Natl. Acad. Sci. U.S.A.* **103,** 2833–2838
74. Northen, H., Paterson, G. K., Constantino-Casas, F., Bryant, C. E., Clare, S., Mastroeni, P., Peters, S. E., and Maskell, D. J. (2010) *Salmonella enterica* serovar typhimurium mutants completely lacking the F_0F_1 ATPase are novel live attenuated vaccine strains. *Vaccine* **28,** 940–949
75. Unden, G., Steinmetz, P., and Degreif-Dünnwald, P. (2014) The aerobic and anaerobic respiratory chain of *Escherichia coli* and *Salmonella enterica*: enzymes and energetics. *EcoSal Plus* 10.1128/ecosalplus.ESP-0005–2013
76. Noda, S., Takezawa, Y., Mizutani, T., Asakura, T., Nishiumi, E., Onoe, K., Wada, M., Tomita, F., Matsushita, K., and Yokota, A. (2006) Alterations of cellular physiology in *Escherichia coli* in response to oxidative phosphorylation impaired by defective F_1-ATPase. *J. Bacteriol.* **188,** 6869–6876
77. Pettersen, E. F., Goddard, T. D., Huang, C. C., Couch, G. S., Greenblatt, D. M., Meng, E. C., and Ferrin, T. E. (2004) UCSF Chimera: a visualization system for exploratory research and analysis. *J. Comput. Chem.* **25,** 1605–1612